HHS Public Access

Author manuscript

Biomaterials. Author manuscript; available in PMC 2021 February 01.

Published in final edited form as:

Biomaterials. 2020 February ; 231: 119667. doi:10.1016/j.biomaterials.2019.119667.

Chemical functionality of Multidomain Peptide Hydrogels governs early host immune response

Tania L. Lopez-Silva[a], **David G. Leach**[a], **Alon Azares**[c], **I-Che Li**[a], **Darren G. Woodside**[c], **Jeffrey D. Hartgerink**[a,b,*]

[a]Department of Chemistry, Rice University, Houston, Texas 77005, USA

[b]Department of Bioengineering, Rice University, Houston, Texas 77005, USA

[c]Department of Molecular Cardiology, Texas Heart Institute, Houston, Texas, 77030, USA

Abstract

Multidomain Peptide (MDP) hydrogels are nanofibrous materials with many potential biomedical applications. The peptide sequence design of these materials offers high versatility and allows for the incorporation of various chemical functionalities into the nanofibrous scaffold. It is known that host response to biomaterials is strongly affected by factors such as size, shape, stiffness, and chemistry. However, there is a lack of fundamental understanding of the host response to different MDP hydrogels. In particular, it is unknown what effect the chemical functionality displayed on the nanofiber has on biological activity. Here we evaluated the early inflammatory host response to four MDP hydrogels displaying amines, guanidinium ions, and carboxylates in a subcutaneous injection model. While all the studied peptide materials possess similar nanostructure and physical properties, they trigger markedly different inflammatory responses. These were characterized by immunophenotyping of the cellular infiltrate using multi-color flow cytometry. The negatively-charged peptides elicit minimal inflammation characterized by tissue-resident macrophage infiltration, fast remodeling, and no collagen deposition or blood vessel formation within the implants. In contrast, the positively-charged peptides are highly infiltrated by immune cells, are remodeled at a slower rate, promote angiogenesis, and result in a high degree of collagen deposition. The presence of dynamic cell phenotypes characterizes the inflammation caused by the lysine-based peptide, including inflammatory monocytes, macrophages, and lymphoid cells, which is seen to be resolving over time. The arginine-based hydrogel shows higher inflammatory response with a persistent and significant infiltration of polymorphonuclear myeloid-derived cells, even ten days after implantation. This understanding of the immune response to peptide biomaterials improves our ability to design effective materials and to tailor their use for specific biomedical applications.

[*]**Corresponding Author**: jdh@rice.edu.

Appendix A. Supplementary data

Supplementary data related to this article can be found at https://doi.org/10.1016/j.biomaterials.2019.x.x.

Data availability

The raw/processed data required to reproduce these findings cannot be shared at this time due to technical or time limitations.

Graphical Abstract.

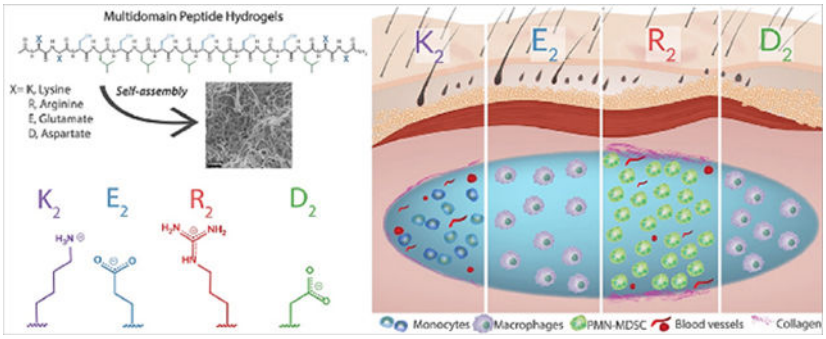

Keywords

Peptide; hydrogel; nanofiber; host response; immune response; inflammation

1. Introduction

A class of peptide-based material that has shown promise in regenerative medicine is the Multidomain Peptide (MDP) [1]. MDPs self-assemble into nanofibrous hydrogels composed of 1% by weight peptide and 99% aqueous buffer. These hydrogels are attractive as biomaterials because they are composed of inherently biocompatible amino acids, and their nanofibrous structure resembles the extracellular matrix, allowing for interaction with cells and complex living systems. The choice of peptide sequence can also modify the bioactivity of these peptide-based materials, and the robust multidomain design offers high versatility as a platform to display different chemical functionalities or biological signals. In aqueous buffers, MDPs form compliant injectable hydrogels that facilitate material implantation, avoiding tissue damage and injury that would be incurred during surgical implantation of a non-injectable biomaterial scaffold [1]. Because of their attractive properties, MDP hydrogels have been studied for different medical applications such as drug and protein delivery, wound healing, cellular encapsulation, and display of bioactive cues [1–7]. Despite the successes and promising results of MDPs in different models, there is a lack of fundamental understanding of the host response to these materials and how the chemical structure of the MDP affects the in vivo response to the peptide hydrogels.

The successful performance of materials in any biological application depends to a large degree on their induced host immune response. That is, the material should efficiently perform its function without eliciting any undesired effects or causing unnecessary damage to the tissue [8]. The host immune response to a vast variety of synthetic and biological-derived materials has been studied [9–11]. Most biomaterials, including PEG [12], polyethylene [13], and crosslinked collagen [14], induce a classical immune response called the foreign body reaction (FBR), resulting in an unresolved chronic inflammation and fibrous encapsulation of the material [15,16]. The FBR is composed of coordinated biological phases that go from an early acute inflammatory response with the presence of immune cells to the formation of granulation tissue, fibrous encapsulation, and the presence of foreign body giant cells [17,18]. It has been found that modifying the biomaterial's

properties or composition, such as chemical functionality, shape, size, and stiffness modulate the severity and outcome of these immune responses [19–23]. For example, in the case of polymeric materials, larger particle sizes and porosity help to reduce the fibrotic response [24,25]; whereas for biologically sourced materials, the origin, processing or crosslinking degree has a significant impact on host response and immunogenicity [14,26,27]. Therefore, it is essential to understand a biomaterial's fundamental interactions with living systems, and how chemical or physical modifications affect them. Such understanding will improve our ability to design biomaterials with specifically tailored immune responses, increasing material efficacy within their desired applications.

The versatile MDP sequence design, generally composed of two different domains, allows for the display of varying chemical functionalities in the ionic charged domain or the amphiphilic domain (Figure 1a) [28,29]. The amphiphilic core of alternating hydrophilic (serine) and hydrophobic (leucine) amino acids or $(SL)_6$, drives the self-assembly into nanofibers, and two flanking domains containing ionic charged amino acids that modulate assembly via charge repulsion and control hydrogelation by the addition of multivalent ions [29,30]. Using this rationale, we have designed diverse MDPs displaying different charge chemical functionalities, for example, positively-charged MDPs, $K_2(SL)_6K_2$ bearing protonated amines and $R_2(SL)_6R_2$ containing guanidinium ions or negatively-charged MDPs such as $E_2(SL)_6E_2$ or $D_2(SL)_6D_2$ displaying carboxylate groups at physiological pH. In previous works, it was observed that the lysine-based peptide, $K_2(SL)_6K_2$, is rapidly infiltrated by host cells when implanted in the subcutaneous space. It was found to degrade over a few weeks while inducing the formation of blood vessels and nerves within and around the implant [31]. These were general and macroscopic observations of the host response to the lysine-based MDP, and thus there is a need for a more detailed evaluation of the host immune response and a comparison to MDPs displaying other chemical functionalities. In this work, we evaluated the early host immune response to four different MDPs: $K_2(SL)_6K_2$, $R_2(SL)_6R_2$, $E_2(SL)_6E_2$ and $D_2(SL)_6D_2$. Hereafter we call these MDPs K_2, R_2, E_2 and D_2 respectively. (Figure 1b, Table S1). The MDPs K_2 and E_2 have been previously reported on by our lab [29,31,32] while MDPs R_2 and D_2 are reported for the first time in this work. We analyze how the chemical functionality and ionic charge of these peptide materials influence the host inflammatory response in a healthy mouse subcutaneous injection model by characterizing the implant microenvironment over time. This assessment provides the knowledge required to tailor the MDP biomaterial designs for diverse applications and according to the desired effects.

2. Materials and methods

2.1 Material preparation and characterization

2.1.1 Peptide synthesis.—All peptides were synthesized using solid-phase peptide synthesis in an Apex Focus XC automated synthesizer (Aapptec) according to the methodology previously reported [29]. Briefly, low-loading Rink Amide MBHA resin (0.32 mmol/g) was used for C-terminal amidation, and N-termini were acetylated before cleavage with a cleavage cocktail of trifluoroacetic acid (TFA) and scavengers. TFA was evaporated, and the peptides were precipitated by trituration with diethyl ether. Peptides were dialyzed

against deionized Milli-Q water for 4-5 days in 100-500 Da MWCO dialysis tubing (Spectra/Por, Spectrum Laboratories Inc. Rancho Dominguez, CA). Peptides were pH-adjusted to 7-7.4, sterile filtered with a 0.2 μm polystyrene filter, frozen, lyophilized and stored at −20°C. Peptide mass and purity were confirmed by mass spectroscopy using an Autoflex MALDI-TOF MS (Bruker Instruments, Billerica, MA) (Figure S1).

2.1.2 Peptide hydrogelation.—Peptides were dissolved in 298 mM sucrose solution in Milli-Q water at a concentration of 2% by weight (20 mg/mL). Peptide solutions were then diluted at a 1:1 ratio with 1X HBSS to promote gelation. The final concentration of the hydrogel was 1% by weight peptide (10 mg/mL) in 149 mM sucrose and 0.5 X HBSS for K_2 and R_2. In the case of E_2 and D_2, $MgCl_2$ was added to the sucrose-HBSS system to a final concentration of 22.5 mM of Mg^{2+} to enhance gelation. This buffer system is isosmotic with physiological conditions.

2.1.3 Circular Dichroism (CD) spectroscopy.—To characterize the secondary structure of all MDPs, peptide solutions of 1% by weight (Molar concentration is included in Table S1) were prepared as described above and analyzed in a CD Jasco J-810 spectropolarimeter (Jasco Inc. Easton, MD) using a 0.01 mm cuvette. Five scans per sample were collected at room temperature from 180 to 250 nm at a speed of 50 nm/min, with a 0.1 nm data pitch.

2.1.4 Attenuated Total Reflectance Fourier Transform Infrared Spectroscopy (ATR-FTIR).—10 μL of the peptide solution described previously were dried under nitrogen flow on a Golden Gate diamond window of an ATR stage. IR spectra were collected using a Jasco FT/IR-660 plus spectrometer (Jasco Inc., Easton, MD) at a 1 cm^{-1} resolution with a 64 scans accumulation. The background was subtracted from all the spectra, and Spectragryph optical spectroscopy software was used for data processing and normalization [33].

2.1.5 Transmission Electron Microscopy (TEM).—Peptide solutions of 0.05 % by weight in Milli-Q water were diluted from a 1% by weight stock solution, 10 mg/mL of peptide in 149 mM sucrose and 0.5X HBSS for K_2 and R_2. Same conditions were used for the stock solution of E_2 and D_2 with the addition of 22.5 mM $MgCl_2$. The peptide solution was spotted on Quantifoil R1.2/1.3 holey carbon films on copper mesh grids and allowed to absorb for 1 min before the excess was blotted. Negative staining was performed using 2% by weight phosphotungstic acid (PTA) solution in Milli-Q water at pH 7. The samples were negatively stained for 5 min in PTA, and then the excess solution was removed. Samples were air dried and imaged at 120 kV and 40K magnification using a JEOL 2010 TEM microscope (JEOL USA Inc., Peabody, MA).

2.1.6 Oscillatory Rheology.—Viscoelastic properties of all peptide hydrogels were analyzed by oscillatory rheology using an AR-G2 rheometer (TA Instruments, New Castle, DE). Peptide hydrogels were prepared as described above and allowed to sit undisturbed for 24 h before the rheology test. 150 μL of 1% by weight hydrogel was transferred from an end-truncated 3 mL syringe onto the rheometer stage. The sample was analyzed using a 12 mm stainless-steel parallel plate set to a 1000 μm gap height. The storage modulus (G') and loss modulus (G") were monitored under various oscillatory strain and frequency as has

been previously described [34]. Strain sweep analysis was performed from 0.01 to 200% strain at a 1 rad/s frequency. A frequency sweep was performed under 1% strain at 0.1-100 rad/s. Shear recovery was performed by applying 1% strain for 20 min, then 200% strain for 1 min and finally 1% strain for 10 min measuring the G' and G" recovery (Figure S2, Table S2).

2.1.7 Scanning Electron Microscopy (SEM).—Peptide hydrogels were prepared as described in section 2.1.5, then dehydrated with a series of ethanol treatment from 30% to 100%. Ethanol was removed by critical point drying using an EMS 850 critical point dryer (Electron Microscopy Sciences, Hatfield, PA). Dried samples were mounted into SEM pucks with the aid of conductive carbon tape and coated with 4-5 nm of gold using a Denton Desk V Sputter system (Denton Vacuum, Moorestown, NJ). Samples were imaged using a JEOL 6500F Scanning Electron Microscope (JEOL, USA Inc., Peabody, MA).

2.2 Evaluation of the host response to peptide hydrogels

2.2.1 In vivo subcutaneous injection model.—All experimental procedures were approved by the Rice University Institutional Animal Care and Use Committee (IACUC) and performed according to the Animal Welfare Act and NIH guidelines for the care and use of laboratory animals. Female C57BL/6 mice from 8 to 12 weeks old were purchased from Charles River Laboratories (Wilmington, MA). Mice were anesthetized using isoflurane (2% carried by oxygen) and maintained on a nose cone with 1.5 - 2% isoflurane. Hair from the dorsal aspect was clipped, the area was cleaned with 70% isopropyl alcohol swabs. Four injections of 100 μL 1% by weight sterile peptide hydrogel were distributed along the dorsal subcutaneous space using a 26-gauge needle, as shown in Figure S3. Animals were euthanized by CO_2 asphyxiation while anesthetized at days 1, 3, 7 or 10 post injection. The dorsal tissue was harvested and processed for flow cytometry or histology.

2.2.2 Tissue processing and staining.—Dorsal tissue from the mice was fixed with 10% neutral buffered formalin, hydrogel implants and skin were trimmed, cut, and processed into paraffin blocks. Tissue was sectioned at 5 μm thickness, deparaffinized, hydrated and stained with hematoxylin and eosin or Masson's trichome using standard procedures. For fluorescent immunostaining, tissue sections were deparaffinized, hydrated and antigens were retrieved by boiling in sodium citrate buffer (10 mM sodium citrate, 0.05% Tween 20 at pH 6.0). Tissues were permeabilized with 0.5% Triton X-100 and blocked with 1% by weight BSA in PBS for 30 min. Tissue slides were incubated overnight at 4°C with rabbit polyclonal anti alpha-smooth muscle actin antibody (1:500 dilution, isotype IgG, Genetex, Cat# GTX100034). Then, samples were rinsed with PBS and incubated for 1 hour with secondary antibody: donkey anti-Rabbit IgG (H+L) Alexa Fluor® 568 (1:500 dilution, Invitrogen). The secondary antibody was rinsed in PBS, followed by mounting with ProLong® Gold Antifade reagent with DAPI (Invitrogen). Tissue Slides were analyzed by confocal fluorescent microscopy using a Nikon A1 Rsi fluorescent confocal microscope (Nikon Instruments, Tokyo, Japan).

2.2.3 Immunophenotyping by flow cytometry

2.2.3.1 Implant harvesting and digestion.: Implants were trimmed from any connective and fat tissue and harvested from the skin. Then, the excised hydrogel implants were rinsed with PBS and weighed. Four implants per mouse were digested together using 5 mL of warmed Liberase™ (medium Thermolysin, 0.2 WU/mL in HBSS, Sigma-Aldrich, Cat# 5401119001) and minced into small pieces. Implants were digested for 30 min at 37°C under mild agitation and pipetting. Digestion medium was neutralized with 25 mL of 1% by weight BSA in Dulbecco's PBS (DPBS) with EDTA (2 mM) and filtered with a 70 μm cell strainer. Cells were pelleted by centrifugation at 1200 rpm for 7 min and resuspended in PBS. Cells were counted with a hemocytometer, and cell concentration was adjusted. For E_2 and D_2, detection of the implants at later time points (Day 7 - 10) was more challenging due to faster degradation and lack of coloration. It is possible that cell counting for or the anionic MDPs also includes cells from the connective tissue; therefore, the cell number showed in this work represents the upper limit of the recruited cell population for these anionic peptides.

2.2.3.2 Sample preparation for flow cytometry.: Cell suspensions with 500,000 to 250,000 cells were added to each tube and diluted 1:1 with FACS Buffer (2% v/v FBS in PBS). Samples were incubated for 5 min with 1 μg anti-CD16/CD32 Fc block antibody (Mouse BD Fc Block, BD Biosciences) at 4°C. Samples were co-stained for 30 min on ice with standard panels of immunophenotyping antibodies (final concentration of 10 μg/mL) as described in Table S3. Then, cells were washed with 1 mL of FACS buffer, centrifuged at 1200 rpm for 7 min and washed again with 1X PBS. Cells were resuspended in 500 μL of PBS and stained with Blue live/dead fixable dead cell stain (Invitrogen) for 30 min on ice. Cells were washed one more time with PBS, pellet by centrifugation and resuspended in 200 μL of PBS. The cell suspension was filtered through a 35 μm strainer and fixed with 200 μL of 2% neutral buffered Formalin in PBS. Samples were analyzed in a BD SORP FACSAria I (BD Biosciences, San Jose, CA). Parameters and settings for the specific panels are shown in Table S4. Data were analyzed using BD FACSDiva 6.1.5 (BD Biosciences), FCS express 5 (De Novo, Los Angeles, CA), and FlowJo v10 (Ashland, OR). For every analysis, a cell only control, a single parameter, and a fluorescent minus one control were used to guide manual gating.

2.2.3.3 T-SNE analysis.: Dimensional reduction and clustering of the flow cytometry data was performed using the t-Distributed Stochastic Neighbor Embedding (tSNE) method. Samples from 5 different animals per peptide or time point were used, and data cleaning was performed by gating singlets, viable cells, live cells, and $CD45^+$ cells (Figure S4). Each sample was downsampled to 5000 $CD45^+$ events, and data were concatenated to a single file. tSNE was performed with the following parameters: 1000 iterations, perplexity value 30, eta value 200, and theta of 0.5. Data for cell populations are displayed according to manual gating and plotted as a function of tSNE X and Y coordinates.

2.2.4 Cytokine quantification.—Cytokines produced by cells within the hydrogel implant were quantified using a cytokine bead array (CBA Mouse Th1/ Th2/ Th17 Cytokine kit, BD Biosciences, Cat#. 560485). Excised implants were washed with cold PBS, cut into

smaller pieces in lysis buffer (Abcam, Cat#. Ab152163) with protease inhibitor cocktail (1% v/v, Sigma-Aldrich, Cat#. P8340). Lysis solution was homogenized and kept on ice for 30 min with intermittent vortexing. Cells were disrupted further with 1 min, 10 pulses sonication using a Microson Ultrasonic Cell Disruptor with a 2 mm microprobe. The cell lysate was centrifuged at 15, 000 rpm for 10 min at 4°C, the supernatant was recovered and used for CBA test.

CBA sample preparation was done according to the manufacturer procedure. Briefly, 50 μL of mixed cytokine capture beads, 50 μL of cytokine standards or unknown sample, and 50 μL of PE detection reagent were added to each tube. Samples were incubated for 2 hours at room temperature and protected from light. Then, samples were washed with 1 mL wash buffer, centrifuged at 200 rcf for 5 min, resuspended in 300 μL of wash buffer and analyzed using a BD LSRII flow cytometer (BD Biosciences) and BD FACSDiva software. Median fluorescent intensity (MFI) was used for the standard curve preparation using an asymmetric sigmoidal five-parameter logistic fit model, and MFI from unknown samples was interpolated from the standard curves.

2.3 Statistical Analysis.

All error bars represent standard deviation unless otherwise stated. Differences between groups for rheological properties, cells per implant, weight, and cytokine quantification were determined using a one-way ANOVA with Tukey's multiple comparisons tests using GraphPad Prism v. 8.0.1. Differences between groups at different times were determined using a two-way ANOVA with Tukey's multiple comparisons test. P-values <0.05 were considered significant. Significance between groups is represented by Greek letters where different letters indicate a significant difference. Significance between the same peptide during different periods is represented by symbols where the same symbol means non-significant difference.

3. Results and discussion

3.1 Multidomain Peptides with different chemical functionalities form nanofibrous injectable hydrogels with similar material properties.

The Multidomain Peptide biomaterials investigated in this study are designed to self-assemble into nanofibers driven by an amphiphilic $(SL)_6$ core, while the charged domains are used to regulate the assembly process and allow for hydrogelation by the addition of buffers containing multivalent ions (e.g., PBS, HBSS, cell culture media, etc.). The versatility of MDP design allows for the formation of materials that display different chemical functionalities and ionic charges such as amines, guanidinium ions, or carboxylic acids. It is known that the host immune response to a biomaterial is affected by its chemistry and different factors, including size, shape, and mechanical properties [19–22,24]. In this study we primary sought to understand the effect of the MDP chemistry on the host response; therefore, we first characterized the structural and mechanical properties of the corresponding peptide biomaterials in order to demonstrate that in general, they have similar material properties.

The secondary structure of all peptides (K_2, R_2, E_2, and D_2) was analyzed using circular dichroism spectroscopy (CD) with 1% by weight peptide solutions in 149 mM sucrose and 0.5X HBSS, and additional 22.5 mM Mg^{2+} for the anionic MDPs, E_2 and D_2. The CD spectra are shown in Figure 2a, which demonstrate that the four different MDPs present a canonical β-sheet secondary structure, represented by a minimum near 218 nm and a maximum near 198 nm. Only minor differences in peak intensity or MRE values are observed, which can be due to subtle differences in the β-sheet backbone caused by the presence of different side chains. As a complementary analysis for the secondary structure, dried peptide films were analyzed by ATR-FTIR (Figure 2b). All peptides show an amide I peak around 1620 cm^{-1} characteristic of a β-sheet structure and a weak peak around 1695 cm^{-1} indicating an antiparallel conformation. These data suggest that all the MDPs have a similar secondary structure of an antiparallel β-sheet despite substitution for diverse amino acids and no significant differences are observed.

Nanofiber formation and nanostructure of all MDPs were studied using negative-stained TEM (Figure 2d). K_2, R_2, E_2, and D_2, self-assemble into long and entangled nanofibers in the presence of multivalent counterions and have analogous nanostructure with similar fiber diameters. When the peptide concentration is 1% by weight, and in the presence of buffers such as HBSS at pH 7, all four peptides form high water-content materials (hydrogels) (Figure 2c–e). SEM of the peptide hydrogels (Figure 2e) reveals a high-density nanofiber network that resembles the fibrous extracellular matrix, a relevant property for biomaterials.

The viscoelastic properties of MDPs were also evaluated using oscillatory rheometry (Figure 2c, Figure S2, and Table S2). The storage modulus (G')/loss modulus (G") ratio validates the formation of hydrogels (G'/G" ≥ 10) for all peptides. The G' values at 1% oscillatory strain in the range of 270-1260 Pa indicate that all peptides form relatively soft hydrogels with comparable material properties, where D_2 has the highest G', and R_2 has the lowest. We observed statistically significant differences between the storage moduli of R_2 in comparison with K_2 and D_2, as well as E_2 being significant softer than D_2. Previous characterization of the rheological properties of K_2 and E_2 derivatives have reported G' values around that range (100-400 Pa) in different buffer systems [6,29], for example a G' of 191 Pa for K_2 in Phosphate Buffer Solution at 1% by weight peptide and 490 Pa for $E_2(SL)_6E_2GRGDS$ in a 17.8 mM Mg^{2+} solution. The relatively larger G' values here reported are due to the addition of sucrose and higher multivalent counterion concentrations, which enhance the gelation properties of these peptides. Despite all these differences in the storage moduli, all four MDP hydrogels form soft compliant hydrogels with relatively low G' values that are less than an order of magnitude different. We hypothesize that the chemical functionality of these peptides will be the major factor determining the host immune response. As we demonstrate in the following sections, the difference in stiffness between the negatively-charged peptides appears to have no impact on the overall host response as both peptides elicit similar immune responses. All the MDP hydrogels are thixotropic and can be easily syringe delivered with the ability to recover around 80% of their initial storage modulus after a shearing event (Table S2). The high recovery property makes these supramolecular biomaterials simple to deliver by injection, allowing for less invasive administration without causing larger tissue damage. Overall, the structural and mechanical data for K_2, R_2, E_2, and D_2 demonstrate that these peptides possess comparable physical properties in terms of

secondary structure, nanostructure, and formation of compliant hydrogels, allowing for a subsequent in vivo assessment of the dominant effect of chemical functionality on the host immune response to this family of peptide biomaterials.

3.2 Chemical functionality and ionic charge of Multidomain Peptides elicit divergent host responses to the material

A murine subcutaneous injection model was used to evaluate the early host immune responses to MDP hydrogels (Figure 3a, Figure S3). This model allows for the determination of the innate responses to all peptides without the complications of disease or injury and is minimally invasive. MDP hydrogels, prepared as described in section 2.1.2, were injected without any cells or exogenous signals and analyzed at different time points. Apparent visual differences are observed even by a gross analysis of the implants three days post-injection (Figure 3b). The positively-charged MDPs, K_2, and R_2 are seen to promote an inflammatory response characterized by a yellow appearance and the presence of blood vessels and connective tissue around the implants. In the case of E_2 and D_2, which are negatively-charged, no coloration, blood vessels or surrounding connective tissue are observed. Visual localization of the E_2 and D_2 implants was achieved by observing the bulge-like presence of the hydrogel boluses.

Histological analysis of implants for all peptides stained with H&E is shown in Figure 4 at day 7 post-injection (implants and close-ups at the center and edges of the implants at day 3, 7 and 10 are shown in Figures S5 to S8). Although the four different peptide hydrogels each present some degree of cellular infiltration after three days, there are significant differences between them. By day 3 the K_2 peptide hydrogel is being homogenously infiltrated by the host cells from the peripheral area towards the core, which is not yet wholly infiltrated. On the other hand, R_2 presents a much more heterogeneous infiltration pattern, with a significantly higher total number of cells within the implant (Figure 3e and Figure S5 to S7) and the formation of distinct “cell pools” containing high densities of cell nuclei. As also seen in K_2, only the peripheral area of R_2 implants is infiltrated by day 3 while the core remains a non-infiltrated cell-free hydrogel. In contrast, MDPs with carboxylate side chains, E_2 and D_2, have a much lower degree of infiltration, and the cells that are present are characterized by possessing a single nucleus and large cell body in contrast with K_2 and R_2 which show cells with different morphologies. By day 7, the core of all the implants has been infiltrated (Figure 4). K_2 again shows homogenous cellular infiltration, while R_2 infiltration is more uniform than early time points some cell pools are still observed throughout the implant in between islets of the hydrogel. At this time point, R_2 implants have a significantly higher number of cells per implant in comparison to K_2, E_2, and D_2 (Figure 3c and Figure 4). At day 10, cellular infiltration remains very similar to day 7 without significant changes in the four different peptides; however, a substantial decrease in implant size is observed in E_2 and D_2 (Figure S5, S6 and S10).

Cellular quantification was performed from digested implants after harvesting from the dorsal aspect of the animals. In the case of K_2 and R_2, the implant blouses were well defined and easier to localize and trim from connective or adipose tissue. However, for the negatively-charged MDPs, E_2, and D_2, localization of the implants at later time points such

as day 7 and day 10 post-injection was more challenging due to the fast degradation and lack of coloration and presence of blood vessels, making difficult trimming or cleaning the implants. In general, R_2 peptide hydrogel promotes the highest cellular infiltration during all studied time points and is observed to keep increasing over time (Figure 3e). On the other hand, K_2 reaches a constant and homogenous cell infiltration by day 7. The negatively-charged MDPs also promote low cellular infiltration in comparison with R_2.

Material remodeling *in vivo* was evaluated by monitoring the excised hydrogel implant weights over time, allowing for comparison of changes in relative mass (Figure 3d–f), and, by histological analysis of the implants. The implant weight of negatively-charged MDPs at day 7 post-injection is much lower compared to the cationic peptides, showing an approximate 85% decrease from the initial hydrogel injection. The small implant weight suggests a faster degradation, low cell infiltration, and low extracellular matrix production within the implant of these anionic peptides, which is also observed during histological analysis (Figure 4, S5 to S8). R_2 implant weight is significantly higher than all the other peptides on day 7 and remains constant through day 1 to 7, showing even a slight increase in weight by day 10 post-injection (Figure 3f). This increase in weight observed for R_2 implants can be attributed not only to a slow material remodeling, but also a higher cell infiltration profile and the presence of more collagen and possible fibrous encapsulation of this peptide as shown Masson's Trichrome staining (Figure S10) and alpha-smooth muscle immunostaining (Figure S14).

Collagen deposition and fibrous encapsulation is part of a normal foreign body response when an implanted material is not being remodeled or induces an adverse interaction with the host [35]. Masson's trichrome staining of implant cross-sections was used to stain collagen in blue and compare this aspect of the immune response to all studied MDPs (Figures S10 to S13). At day 3, only native collagen from the subcutaneous tissue is observed around the peripheral area of all the peptide implants. By day 3, the positively-charged MDPs have collagen deposition within the implant and in the implant-connective tissue interface. Seven days post-injection, a higher level of collagen deposition inside and around K_2 is observed as well as the presence of small blood vessels (Figure S14–S16). This collagen deposition is a sign of implant remodeling by the infiltrating cells. R_2 also presents a strong blue stain around and within the implant as well as blood vessels in the peripheral area. At day 10, K_2 remodeling continues, and the hydrogel contains more collagen within the implant. As previously mentioned, R_2 implants present more dark-blue collagen, and signs of fibrous encapsulation can be observed by the formation of a thicker collagen layer with blood vessels and fibrotic cells surrounding the implant. This encapsulation can be observed as well by immunostaining with α-smooth muscle actin, which is present in myofibroblast cells (Figure S14–S17). While this fibrous encapsulation observed for R_2 is relatively modest, it is the first time we have observed this response for any MDP hydrogel. In the case of E_2 and D_2, collagen deposition remains similar to native extracellular tissue, the materials degrade considerably while being infiltrated and remodeled, and there is no visible presence of blood vessels among the different time points (Figure S14).

These histological observations suggest that the chemical and material differences between the four MDPs are influencing the interacting cell populations *in vivo.* The hydrogels can be

grouped into two categories of peptide materials. Within the first group are the highly cell-infiltrated and slow remodeling cationic lysine or arginine materials, K_2 and R_2, and in the second group, the minimally infiltrated and fast degrading anionic aspartate and glutamate materials, E_2 and D_2. There appear to be interesting differences in the host response induced by K_2 and R_2, while E_2 and D_2 appear quite similar overall. The negatively-charged MDPs seem to be non-immunogenic and do not provoke inflammation upon implantation, which has been observed before in glutamate containing peptides [36]. It is also known that positively-charged agents such as Poly-D-Lysine or Poly-L-Lysine can be used to facilitate cell attachment to materials in cell culture [37,38]. It was therefore not surprising that the cationic MDPs used in this study resulted, in general, in greater observed material-to-cell interaction compared to the anionic hydrogels.

It is evident that K_2 and R_2 initiate a different host inflammatory response compared to E_2 and D_2. It has been shown in the literature that peptides and materials containing high densities of lysine or arginine residues can possess cytotoxic effects [39–42]. The mechanism of this cytotoxicity involves association with the negatively charged cell membrane via electrostatic interactions and hydrogen bonding, resulting in some degree of membrane disruption and cell lysis [43,44]. Such cytotoxicity can be more pronounced in arginine-bearing peptides than those with lysine likely due to stronger intermolecular interactions between the arginine side chains and cell membranes, though cytotoxicity has long been observed with both types of cationic residues [45,46]. This suggests that the K_2 and R_2 MDPs may both result in some degree of cell death or damage upon initial implantation *in vivo,* which stimulates a stronger inflammatory immune response from the host. In the case of K_2, this acute inflammatory response seems to resolve relatively quickly, with cell infiltration proceeding in a homogenous manner over the initial 10 days, and the entire implant being fully infiltrated with interacting cell populations. In other publications using K_2, the host inflammatory response to K_2 shown to be beneficial in regenerative applications such as wound healing, promoting the recruitment of repairing cells and accelerating the formation of granulation tissue within the wound bed [3]. Such observed wound healing properties of K_2 are consistent with our observations of an acute but resolvable inflammatory response from this peptide material in this study. R_2 results appear to be a higher inflammatory response that does not resolve over 10 days but continues to increase, suggesting a prolonged and unresolved inflammatory response. This conclusion is consistent with the observations of increased cell numbers and implant weight for R_2 hydrogels even at later time points, and increased collagen deposition and beginnings of a fibrous encapsulation of R_2 implants as the host attempts to wall off a foreign body. These results may be explainable in terms of increased arginine side-chain cytotoxicity to interacting cell populations. While these histological observations are useful and allow for one degree of interpretation of the properties of these materials, a more detailed quantification of the immune cell populations infiltrating these peptide biomaterials would give a better idea of the different inflammatory responses generated.

3.3 Immune cell phenotype is determined by the chemical functionality of MDP hydrogels

Innate immune cells are the first responders to implantation of biomaterials and their interaction with the scaffold will determine the degree of the host response that is evoked

[47]. Therefore, the phenotype characterization of the phenotype of the cellular infiltrate can provide relevant insights about the inflammatory response to the different MDP hydrogels studied herein. To identify the cell types that infiltrate each type of MDP hydrogel, we performed multi-color flow cytometry analysis on the implants for myeloid and lymphoid cells (Table S3–S4 and Figure S18–S20). The panel designs primarily focused on analyzing the presence of inflammatory Ly6C^{high} or Ly6C ^{med} monocytes (CD45^{+} CD11b^{+} Gr-1^{+} Ly6C$^{high\text{-}med}$) [48,49], polymorphonuclear myeloid-derived suppressor cells or PMN-MDSCs (CD45^{+} CD11b^{+} Gr-1^{+} Ly6C$^{low\text{-}neg}$)[50–52], macrophages (CD45^{+} CD11b^{+} Gr-1^{neg} F4/80^{+}) [53,54], natural killer cells (CD45^{+} CD11b^{neg} NK1.1^{+}) [55,56], T-cells (CD45^{+} CD3e^{+} CD4^{+} or CD8a^{+}) [57] and B-cells (CD45^{+} CD19^{+}) [58]. The gating strategy for both panels and instrument parameters are shown in the supporting information (Figures S18–19). Implants of all four different peptide hydrogels seven days post-injection were digested, and the single cell suspensions were analyzed by flow cytometry. Figure 5a shows the t-SNE visualization of diverse cell clusters (cell types) obtained for the myeloid panel for all the MDP hydrogels. As expected from earlier histological observations, E_2 and D_2 present a very similar clustering pattern demonstrating that the negatively-charged MDPs induce a highly similar immune response to each other and are being infiltrated by a broadly similar cell phenotype. In the case of the positively-charged MDPs, the evoked inflammatory response of each peptide induces the recruitment of immune cells resulting in distinct cell clustering different from the negatively-charged MDPs and each other.

As expected, the major population infiltrating the MDP materials are immune cells (CD45^{+} or leukocytes), which correspond to around 80% or more of the live cells by day 7 (Figure 5b). From this leukocyte population, most of the cells (>80%) express CD11b, a common marker present in immune cells from the myeloid origin (Figure 5c). A thorough analysis of the myeloid markers expressed in these cells revealed the presence of characteristic immune cells for each peptide. K^2 is mostly infiltrated by monocytes, macrophages, and a few PMN-MDC cells on day 7 and a significant amount of non-myeloid cells (CD45^{+} CD11b^{neg}) (Figure 5d and 5e). On the other hand, R_2 is infiltrated at day 7, mainly by PMN-MDSCs and macrophages (Figure 5d and 5e). These myeloid cells are responsible for orchestrating inflammatory responses and tissue repair, but can also be responsible for prolonged chronic inflammatory reactions [47,59]. Further exploration of these cells and phenotype progression over time will be discussed in section 3.4.

The immunophenotyping of the infiltrating cells for the negative MDPs, E_2, and D_2, demonstrates a high fraction of F4/80^{+} macrophages, which are consistent with the cell morphology observed in histology. No PMN-MDSC or monocytes are observed in these materials, suggesting that E_2 and D_2 do not induce a pro-inflammatory response and are infiltrated and degraded by tissue-resident macrophages [60,61]. These cells have high phagocytic activity, are responsible for controlling homeostasis in the dermal tissue, and can activate a pro or anti-inflammatory response [61]. The low cellular infiltration, lack of blood vessels, and collagen deposition and fast implant remodeling indicate that the carboxylate groups displayed by these MDPs endow the material with low immunogenicity and do not provoke a pro-inflammatory response. The low immunogenicity of negatively-charged glutamate-displaying peptides has been previously studied, and it was found that these peptides are not taken up and processed by antigen presenting cells and thus do not activate

T-cell and B-cell responses and [36]. These observations can explain the lack of pro-inflammatory responses provoked by E_2 and D_2, which are promising properties for applications in which biomaterial evasion of the immune response is desired. Due to the low number of cells that infiltrate E_2 and D_2 and the rapid size reduction of these hydrogels in vivo, flow cytometry analysis could mainly be feasibly performed at day 7 post-injection. However, preliminary flow data at day 3 post-injection (Figure S20) and histological observations indicate that $CD45^+$ $CD11b^+$ $Gr\text{-}1^{neg}$ $F4/80^+$ macrophages represent around 90% of the cell population infiltrating the anionic peptides at this time point.

3.4 K_2 promotes a short-term inflammatory response while R_2 induces a more prolonged inflammation

It is known that acute inflammation is necessary for a favorable wound healing response and tissue remodeling, particularly after biomaterial implantation [62,63]. This phase of inflammation last for less than a week and is characterized by an orchestrated communication between different cells. Initially, granulocytes or PMN-MDSCs, resident macrophages, and monocytes interact with foreign material and initiate phagocytosis and recruitment of other inflammatory cells. As the inflammatory cascade progresses, macrophages start the degradation and remodeling of the material leading towards inflammation resolution and wound healing. On the other hand, if phagocytic cells are unsuccessful in clearing and remodeling tissue, and there is a prolonged presence of granulocytes or PMN-MDSCs, it could lead to chronic inflammation [64].

To further asses the type of response elicited by the two pro-inflammatory MDP hydrogels, K_2 and R_2, we characterized the cellular infiltrate at day 1, 3, 7, and 10 post-injection. A t-SNE visualization of the cell clusters present in K_2 implants (Figure 6a) shows a different clustering pattern from day 1 to day 7, revealing a dynamic change of phenotypes of recruited cells over this time. Day 7 and day 10 post-injection have similar clusters indicating the consistent presence of similar cells. At day 1, inflammatory and circulating monocytes ($CD45^+$ $CD11b^+$ $Gr\text{-}1^+$ $Ly6C^{high}$ and $CD45^+$ $CD11b^+$ $Gr\text{-}1^+$ $Ly6C^{med}$, respectively), macrophages ($CD45^+$ $CD11b^+$ $Gr\text{-}1^{neg}$ $F4/80^+$), and PMN-MDSC ($CD45^+$ $CD11b^+$ $Gr\text{-}1^+$ $Ly6C^{low\text{-}neg}$) are the majority of infiltrated cells (Figure 6c). These cells are responsible for the initiation and progression of the acute inflammatory response to the biomaterial. Natural killer cells with $CD45^+$ $CD11b^{neg}$ $NK1.1^+$ phenotype are also observed on day 1, which are known to promptly secrete chemokines and cytokines to attract other cells types [65]. By day 3, a large percentage of inflammatory monocytes $CD45^+$ $CD11b^+$ $Gr\text{-}1^+$ $Ly6C^{high}$ are observed, and this correlates with the formation of new vasculature around the implant (Figure 3b and Figure S14) [66]. At day 7, macrophages, monocytes, and other leukocytes ($CD45^+$ cells) are the main cell phenotype present in K_2 implants. There was no significant change in the immune cells at day 7 and day 10 in the implants, suggesting that the acute immune response provoked by the lysine-based peptide hydrogel may be stabilizing. From the non-myeloid cell population, CD3e mature T-cells and CD19 B cells are present particularly at later time points (Day 7 and Day 10) as shown in Figure S21. At day 7, most of the CD19 positive cells express CD11b myeloid marker, which is a marker for B1 cells. These cells are part of the innate and adaptive host responses which react rapidly to inflammatory signals and are capable of clearing apoptotic cells and secrete anti-

inflammatory cytokines [67]. On the other hand, CD3e mature T lymphocytes are present in a lower percentage that increases by day 10. This suggests the progression of inflammation and a degree of immunogenicity from the K^2 peptide hydrogel.

These observations, together with the decrease in implant weight, implant remodeling, and relatively constant cell number within the implant suggest that the inflammation caused by K_2 implantation is resolving over time and cells start remodeling the material. Supported by the known angiogenic and neurogenic properties of the K_2 peptide that have been previously reported [31], our results confirm that this peptide is a promising biomaterial for regenerative applications because it elicits an acute inflammatory response that promotes vascularization, innervation, and tissue remodeling, all necessary elements for wound healing and tissue regeneration. The capacity of this peptide material to recruit adaptive immune cells such as T cells, B cells, and NK cells also make it suitable for immunotherapy approaches.

In the case of R_2, a less dynamic response is observed, and similar t-SNE clustering is seen throughout all studied time points (Figure 6b). Immunophenotyping of the infiltrating cells revealed a consistent percentage of $CD45^+$ $CD11b^+$ $Gr\text{-}1^+$ $Ly6C^{low/neg}$ cells that can be described as PMN-MDSC as well as $CD45^+$ $CD11b^+$ $Gr\text{-}1^{neg}$ $F4/80^+$ macrophages (Figure 6d). As mentioned before, R_2 implants do not decrease in weight over time and are observed to promote increased cellular infiltration, which indicates that inflammation may not be resolving even at ten days post-injection. The maintenance of recruited PMN-MDSC suggests the development of an immune response that could lead to chronic inflammation and fibrous encapsulation [21,47].

3.5 Pro-inflammatory cytokines are present in K_2 and R_2 implants

The inflammatory response is controlled by chemical signals or cytokines that are secreted by immune cells to induce pro or anti-inflammatory responses. The presence and levels of cytokines give a perspective of the local inflammatory environment and response to each peptide hydrogel. Quantification of pro-inflammatory cytokines such as Tumor Necrosis Factor (TNF), IL-6, IL-4, and INF-γ at day 1, 3, 7, and 10 post-injection is shown in Figure 7 and Figure S22. All studied cytokines are present in the positively-charged MDPs, K_2, and R_2, but not detectable in the negatively-charged MDPs, E_2, and D_2. The inflammatory response provoked by K_2 and R_2 is characterized by the presence TNF from day 1 to day 10, with the highest concentration being at day 3. Data suggest that 3 days post-injection is the peak of inflammation in both peptide hydrogels, and then the concentration of TNF decreases by day 7 and remains constant at day 10. TNF is a potent pro-inflammatory cytokine that stimulates the inflammatory response [68], and the high concentration of this cytokine in comparison with typical blood serum values (> 10 pg/mL) [69] indicates the initial inflammation caused by the implantation of these peptides. This cytokine is produced mainly by activated macrophages but also by monocytes and NK cells [70], which correspond to the main cell types found in the cellular infiltrate for K_2 and R_2. Another detected cytokine in the implant lysate is IL-6, a regulating cytokine that has an important function in tissue repair and in early time points is considered a pro-inflammatory cytokine secreted by macrophages and monocytes [14,68]. The highest concentration of IL-6 was

present at day 1 in the R_2 implant lysate of around 600 pg/mL in comparison with reported low blood serum levels (> 10 pg/mL) [69]. The concentration of this cytokine significantly decreased over time in the R_2 implants. A similar trend is observed for the lysine-based MDP, K_2, where the concentration of IL-6 is high at day 1 but decreases by day 7. However, K_2 implants have a lower concentration of IL-6 by day 1 and 3 than R_2 implants, supporting the formation of a stronger inflammatory response in R_2 that is consistent with previous observations.

3.6 Cells expressing mesenchymal stem cell markers are present in the inflammatory response to MDP hydrogels

The characterization of the immune cells that infiltrate the MDP hydrogels revealed a significant myeloid population with diverse phenotypes. However, there is a small percentage of cells that do not express the leukocyte common antigen CD45 and myeloid marker CD11b. In order to identify these cells, a stem cell panel for hematopoietic and mesenchymal stem cells (MSCs) was performed (Figure S23, Table S4) as it has been reported that stem cells are recruited during biomaterial implantation for immunomodulation and tissue repair [71,72]. At seven days post-implantation, cells with the phenotype $CD45^{neg}$ $CD11b^{neg}$ $Sca\text{-}1^{+}$ are present in the four different MDP implants (Figure 8). These cells also express $CD29^{+}$, and the majority are negative for CD105 (endoglin) (Figure S23), which are common markers for MSCs [72]. These data suggest the presence of $CD105^{neg}$ MSCs, which are known to be present in the subcutaneous tissue of mice and have a high propensity to differentiate into adipose tissue [73]. The immunomodulatory properties and capacity to secrete anti-inflammatory cytokines indicate that these cells are attracted to the biomaterial implantation site as part of the inflammatory response to regulate and promote tissue repair, particularly at later time points [74]. These $CD105^{neg}$ MSCs are present in a higher percentage in the negatively-charged MDPs, which suggest that they are involved in depressing the inflammatory response to these peptide materials as part of their immunomodulatory properties.

4. Conclusions

We have shown that the chemical functionality displayed by the charged domains of Multidomain peptides has a high impact on the host immune response to the peptide hydrogel. These results are summarized in Table 1. In general, all studied MDPs possess similar nanostructural and mechanical properties. Their chemical design results in a β-sheet conformation that facilitates the formation of peptide nanofibers, which are then stabilized and physically crosslinked by the addition of multivalent counterions. As a result, all MDPs form soft ECM-like peptide hydrogels that do not differ considerably in their viscoelastic properties and can be easily injected *in vivo*. The versatility of the MDP design allowed the display of different chemical functionalities at the nanofiber surface and thus endowing the resulting biomaterials with diverse biological properties and potential applications.

Deprotonated carboxylic acids present in glutamate and aspartate-based MDPs, E_2, and D_2 evoke a minimal inflammatory response characterized by the low infiltration of tissue-resident macrophages, low inflammatory cytokine content, the absence of vasculature and

collagen deposition around and within the implant and an increased rate of degradation. These responses can be of great advantage for applications that do not require immunological reactions or unnecessary inflammation such as delivery vehicles for cells, small molecules, or proteins. On the other hand, the lysine-based MDP K_2 bearing protonated amines induces an acute inflammatory response that resolves over time. This response is characterized by the presence of acute immune cells, such as inflammatory monocytes, in the first few days post-injection that develop into macrophages by day 7. K_2 implants promote vascularization and are remodeled by the host cells with collagen deposition observed in tandem with material degradation. Overall, the K_2 peptide hydrogel elicits an acute inflammatory response required for a normal wound healing process, making this MDP hydrogel promising for tissue regeneration applications. The arginine-based MDP R_2 displaying guanidinium ions provokes a pro-inflammatory response that is not observed to resolve at ten days post-injection. This material recruits PMN-MDSCs, which remain in the implant over all time points. High vasculature and collagen deposition are also observed around and within the implant, which transitions into the early development of a fibrous capsule. The host response caused by R_2 could inhibit wound healing and tissue regeneration, but its highly inflammatory response could be advantageous for immunostimulatory applications such as cancer immunotherapy.

This work describes the first in-depth characterization of early host immune response to a diverse family of Multidomain peptide hydrogels, establishing the basis of biocompatibility and immune responses to positively or negatively-charged peptide hydrogels. The greater understanding of the divergent responses to peptide hydrogels will allow for guided material design and will facilitate more successful selection of ideal materials for diverse tissue engineering, therapeutic delivery, and regenerative medicine applications.

Supplementary Material

Refer to Web version on PubMed Central for supplementary material.

Acknowledgements

This work was supported in part by funding from the NIH (DE021798) and the Welch Foundation (C1557). T.L.L-S. was supported by the Mexican National Council for Science and Technology (CONACyT) Ph.D. Scholarship Program (678341). D.G.L. was supported by the NSF Graduate Research Fellowship Program under Grant No. 1842494. I.L. was supported by the Stauffer-Rothrock Fellowship. The authors acknowledge the support from the Flow Cytometry Core at the Texas Heart Institute (THI) and the BD Biosciences Immunology research grant.

References

[1]. Moore AN, Hartgerink JD, Self-Assembling Multidomain Peptide Nanofibers for Delivery of Bioactive Molecules and Tissue Regeneration, Acc. Chem. Res. 50 (2017) 714–722. 10.1021/acs.accounts.6b00553. [PubMed: 28191928]

[2]. Leach DG, Dharmaraj N, Piotrowski SL, Lopez-Silva TL, Lei YL, Sikora AG, Young S, Hartgerink JD, STINGel: Controlled release of a cyclic dinucleotide for enhanced cancer immunotherapy, Biomaterials. 163 (2018) 67–75. 10.1016/j.biomaterials.2018.01.035. [PubMed: 29454236]

[3]. Carrejo NC, Moore AN, Lopez Silva TL, Leach DG, Li IC, Walker DR, Hartgerink JD, Multidomain Peptide Hydrogel Accelerates Healing of Full-Thickness Wounds in Diabetic Mice,

ACS Biomater. Sci. Eng. 4 (2018) 1386–1396. 10.1021/acsbiomaterials.8b00031. [PubMed: 29687080]

[4]. Li IC, Moore AN, Hartgerink JD, “Missing Tooth” Multidomain Peptide Nanofibers for Delivery of Small Molecule Drugs, Biomacromolecules. 17 (2016) 2087–2095. 10.1021/acs.biomac.6b00309. [PubMed: 27253735]

[5]. Wickremasinghe NC, Kumar VA, Hartgerink JD, Two-Step Self-Assembly of Liposome-Multidomain Peptide Nanofiber Hydrogel for Time-Controlled Release, Biomacromolecules. 15 (2014) 3587–3595. 10.1021/bm500856c. [PubMed: 25308335]

[6]. Bakota EL, Wang Y, Danesh FR, Hartgerink JD, Injectable multidomain peptide nanofiber hydrogel as a delivery agent for stem cell secretome, Biomacromolecules. 12 (2011) 1651–1657. 10.1021/bm200035r. [PubMed: 21417437]

[7]. Leach DG, Newton JM, Florez MA, Lopez-silva TL, Jones AA, Young S, Sikora AG, Hartgerink D, Drug-Mimicking Nanofibrous Peptide Hydrogel for Inhibition of Inducible Nitric Oxide Synthase, ACS Biomater. Sci. Eng. (2019). 10.1021/acsbiomaterials.9b01447.

[8]. Ratner BD, Chapter 3 - The Biocompatibility of Implant Materials, in: S.F.B.T.-H.R. to Badylak B (Ed.), Academic Press, Oxford, 2015: pp. 37–51. 10.1016/B978-0-12-800196-7.00003-7.

[9]. Anderson J, Cramer S, Perspectives on the Inflammatory, Healing, and Foreign Body Responses to Biomaterials and Medical Devices, Elsevier Inc., 2015 10.1016/B978-0-12-800196-7.00002-5.

[10]. Lopresti ST, Brown BN, Host Response to Naturally Derived Biomaterials, Elsevier Inc., 2015 10.1016/B978-0-12-800196-7.00004-9.

[11]. Corradetti B, ed., The Immune Response to Implanted Materials and Devices, Springer International Publishing, Cham, 2017 10.1007/978-3-319-45433-7.

[12]. Lynn AD, Blakney AK, Kyriakides TR, Bryant SJ, Temporal progression of the host response to implanted poly(ethylene glycol)-based hydrogels, J. Biomed. Mater. Res. - Part A. 96 A (2011) 621–631. 10.1002/jbm.a.33015.

[13]. Gibon E, Córdova LA, Lu L, Lin TH, Yao Z, Hamadouche M, Goodman SB, The biological response to orthopedic implants for joint replacement. II: Polyethylene, ceramics, PMMA, and the foreign body reaction, J. Biomed. Mater. Res. - Part B Appl. Biomater. 105 (2017) 1685–1691. 10.1002/jbm.b.33676. [PubMed: 27080740]

[14]. Delgado LM, Bayon Y, Pandit A, Zeugolis DI, To Cross-Link or Not to Cross Link? Cross-Linking Associated Foreign Body Response of Collagen-Based Devices, Tissue Eng. Part B Rev. 21 (2015) 298–313. 10.1089/ten.teb.2014.0290. [PubMed: 25517923]

[15]. Anderson JM, Rodriguez A, Chang DT, Foreign body reaction to biomaterials, Semin. Immunol. 20 (2008) 86–100. 10.1016/j.smim.2007.11.004. [PubMed: 18162407]

[16]. Anderson JM, Biological Responses To Materials, Annu. Rev. Mater. Res. 31 (2001) 81–110. 10.1146/annurev.matsci.31.1.81.

[17]. Babensee JE, Anderson JM, McIntire LV, Mikos AG, Host response to tissue engineered devices, Adv. Drug Deliv. Rev. 33 (1998) 111–139. 10.1016/S0169-409X(98)00023-4. [PubMed: 10837656]

[18]. Jones K, Fibrotic Response to Biomaterials and all Associated Sequence of Fibrosis, Elsevier Inc., 2015 10.1016/B978-0-12-800196-7.00009-8.

[19]. Boddupalli A, Zhu L, Bratlie KM, Methods for Implant Acceptance and Wound Healing: Material Selection and Implant Location Modulate Macrophage and Fibroblast Phenotypes, Adv. Healthc. Mater. 5 (2016) 2575–2594. 10.1002/adhm.201600532. [PubMed: 27593734]

[20]. Kamath S, Bhattacharyya D, Padukudru C, Timmons RB, Tang L, Surface chemistry influences implant-mediated host tissue responses, J. Biomed. Mater. Res. - Part A. 86 (2008) 617–626. 10.1002/jbm.a.31649.

[21]. Sadtler K, Wolf MT, Ganguly S, Moad CA, Chung L, Majumdar S, Housseau F, Pardoll DM, Elisseeff JH, Divergent immune responses to synthetic and biological scaffolds, Biomaterials. 192 (2018) 405–415. 10.1016/j.biomaterials.2018.11.002. [PubMed: 30500722]

[22]. Lebre F, Sridharan R, Sawkins MJ, Kelly DJ, O’Brien FJ, Lavelle EC, The shape and size of hydroxyapatite particles dictate inflammatory responses following implantation, Sci. Rep. 7 (2017) 1–13. 10.1038/s41598-017-03086-0. [PubMed: 28127051]

[23]. Corradetti B, Taraballi F, Corbo C, Cabrera F, Pandolfi L, Minardi S, Wang X, Van Eps J, Bauza G, Weiner B, Tasciotti E, Immune tuning scaffold for the local induction of a pro-regenerative environment, Sci. Rep. 7 (2017) 1–13. 10.1038/s41598-017-16895-0. [PubMed: 28127051]

[24]. Veiseh O, Doloff JC, Ma M, Vegas AJ, Tam HH, Bader AR, Li J, Langan E, Wyckoff J, Loo WS, Jhunjhunwala S, Chiu A, Siebert S, Tang K, Hollister-Lock J, Aresta-Dasilva S, Bochenek MA, Mendoza-Elias JE, Wang Y, Qi M, Lavin DM, Chen M, Dholakia N, Thakrar R, Lacik I, Weir GC, Oberholzer J, Greiner DL, Langer R, Anderson DG, Size- and shape-dependent foreign body immune response to materials implanted in rodents and non-human primates., Nat. Mater. 14 (2015) 643–51. 10.1038/nmat4290. [PubMed: 25985456]

[25]. Fukano Y, Usui ML, Underwood RA, Isenhath S, Marshall AJ, Hauch KD, Ratner BD, Olerud JE, Fleckman P, Epidermal and dermal integration into sphere-templated porous poly(2-hydroxyethyl methacrylate) implants in mice, J. Biomed. Mater. Res. - Part A. 94 (2010) 1172–1186. 10.1002/jbm.a.32798.

[26]. Aamodt JM, Grainger DW, Extracellular matrix-based biomaterial scaffolds and the host response, Biomaterials. 86(2016) 68–82. 10.1016/j.biomaterials.2016.02.003. [PubMed: 26890039]

[27]. Morris AH, Stamer DK, Kyriakides TR, The host response to naturally-derived extracellular matrix biomaterials, Semin. Immunol. 29 (2017) 72–91. 10.1016/j.smim.2017.01.002. [PubMed: 28274693]

[28]. Bakota EL, Sensoy O, Ozgur B, Sayar M, Hartgerink JD, Self-assembling multidomain peptide fibers with aromatic cores., Biomacromolecules. 14 (2013) 1370–8. 10.1021/bm4000019. [PubMed: 23480446]

[29]. Aulisa L, Dong H, Hartgerink JD, Self-assembly of multidomain peptides: Sequence variation allows control over cross-linking and viscoelasticity, Biomacromolecules. 10 (2009) 2694–2698. 10.1021/bm900634x. [PubMed: 19705838]

[30]. Dong H, Paramonov SE, Aulisa L, Bakota EL, Hartgerink JD, Self-assembly of multidomain peptides: Balancing molecular frustration controls conformation and nanostructure, J. Am. Chem. Soc. 129 (2007) 12468–12472. 10.1021/ja072536r. [PubMed: 17894489]

[31]. Moore AN, Lopez Silva TL, Carrejo NC, Origel Marmolejo CA, Li IC, Hartgerink JD, Nanofibrous peptide hydrogel elicits angiogenesis and neurogenesis without drugs, proteins, or cells, Biomaterials. 161 (2018) 154–163. 10.1016/j.biomaterials.2018.01.033. [PubMed: 29421552]

[32]. Lopez-Silva TL, Leach DG, Li I-C, Wang X, Hartgerink JD, Self-Assembling Multidomain Peptides: Design and Characterization of Neutral Peptide-Based Materials with pH and Ionic Strength Independent Self-Assembly, ACS Biomater. Sci. Eng. 5 (2018) 977–985. 10.1021/acsbiomaterials.8b01348. [PubMed: 31404449]

[33]. Menges F, Spectragryph - optical spectroscopy software, (2017) Version 1.2.7. http://www.effemm2.de/spectragryph/.

[34]. Li IC, Hartgerink JD, Covalent Capture of Aligned Self-Assembling Nanofibers, J. Am. Chem. Soc. 139 (2017) 8044–8050. 10.1021/jacs.7b04655. [PubMed: 28581735]

[35]. Rujitanaroj PO, Jao B, Yang J, Wang F, Anderson JM, Wang J, Chew SY, Controlling fibrous capsule formation through long-term down-regulation of collagen type i (COL1A1) expression by nanofiber-mediated siRNA gene silencing, Acta Biomater. 9 (2013) 4513–4524. 10.1016/j.actbio.2012.09.029. [PubMed: 23036951]

[36]. Wen Y, Waltman A, Han H, Collier JH, Switching the Immunogenicity of Peptide Assemblies Using Surface Properties, ACS Nano. 10 (2016) 9274–9286. 10.1021/acsnano.6b03409. [PubMed: 27680575]

[37]. Mazia D, Schatten G, Sale W, Adhesion of cells to surfaces coated with polylysine. Applications to electron microscopy, J. Cell Biol. 66 (1975) 198 10.1083/jcb.66.1.198. [PubMed: 1095595]

[38]. Kim YH, Baek NS, Han YH, Chung M-A, Jung S-D, Enhancement of neuronal cell adhesion by covalent binding of poly-d-lysine, J. Neurosci. Methods. 202 (2011) 38–44. 10.1016/j.jneumeth.2011.08.036. [PubMed: 21907237]

[39]. Shoji HM Shima Toshior Iwamoto, Heiishi Sakai, Antimicrobial action of ε-poly-L-lysine , J. Antibiot. (Tokyo). 37 (1984) 1449–1455. [PubMed: 6392269]

[40]. Salick DA, Kretsinger JK, Pochan DJ, Schneider JP, Inherent Antibacterial Activity of a Peptide-Based β-Hairpin Hydrogel, J. Am. Chem. Soc. 129 (2007) 14793–14799. 10.1021/ja076300z. [PubMed: 17985907]

[41]. Veiga AS, Sinthuvanich C, Gaspar D, Franquelim HG, Castanho MARB, Schneider JP, Arginine-rich self-assembling peptides as potent antibacterial gels, Biomaterials. 33 (2012) 8907–8916. 10.1016/j.biomaterials.2012.08.046. [PubMed: 22995710]

[42]. Gabriel GJ, Som A, Madkour AE, Eren T, Tew GN, Infectious disease: Connecting innate immunity to biocidal polymers, Mater. Sci. Eng. R Reports. 57 (2007) 28–64. 10.1016/j.mser.2007.03.002.

[43]. Li P, Poon YF, Li W, Zhu H-Y, Yeap SH, Cao Y, Qi X, Zhou C, Lamrani M, Beuerman RW, Kang E-T, Mu Y, Li CM, Chang MW, Jan Leong SS, Chan-Park MB, A polycationic antimicrobial and biocompatible hydrogel with microbe membrane suctioning ability, Nat. Mater. 10 (2010) 149 10.1038/nmat2915. [PubMed: 21151166]

[44]. Schmidt NW, Mishra A, Lai GH, Davis M, Sanders LK, Tran D, Garcia A, Tai KP, McCray PB, Ouellette AJ, Selsted ME, Wong GCL, Criterion for Amino Acid Composition of Defensins and Antimicrobial Peptides Based on Geometry of Membrane Destabilization, J. Am. Chem. Soc. 133 (2011) 6720–6727. 10.1021/ja200079a. [PubMed: 21473577]

[45]. Chan DI, Prenner EJ, Vogel HJ, Tryptophan- and arginine-rich antimicrobial peptides: Structures and mechanisms of action, Biochim. Biophys. Acta - Biomembr. 1758 (2006) 1184–1202. 10.1016/j.bbamem.2006.04.006.

[46]. de Leeuw E, Rajabi M, Zou G, Pazgier M, Lu W, Selective arginines are important for the antibacterial activity and host cell interaction of human α-defensin 5, FEBS Lett. 583 (2009) 2507–2512. 10.1016/j.febslet.2009.06.051. [PubMed: 19589339]

[47]. Selders GS, Fetz AE, Radic MZ, Bowlin GL, An overview of the role of neutrophils in innate immunity, inflammation and host-biomaterial integration, Regen. Biomater. 4 (2017) 55–68. 10.1093/rb/rbw041. [PubMed: 28149530]

[48]. Ginhoux F, Jung S, Monocytes and macrophages: Developmental pathways and tissue homeostasis, Nat. Rev. Immunol. 14 (2014) 392–404. 10.1038/nri3671. [PubMed: 24854589]

[49]. Dillon MJ, Leenen PJM, Nikolic T, Stehling M, Sunderkotter C, Drevets DA, van Rooijen N, Subpopulations of Mouse Blood Monocytes Differ in Maturation Stage and Inflammatory Response, J. Immunol. 172 (2014) 4410–4417. 10.4049/jimmunol.172.7.4410.

[50]. Lee PY, Wang J-X, Dascher CC, Nigrovic PA, Parisini E, Ly6 family proteins in neutrophil biology, J. Leukoc. Biol. 94 (2013) 585–594. 10.1189/jlb.0113014. [PubMed: 23543767]

[51]. Albina JE, Connolly MD, Thomay AA, Reichner JS, Daley JM, Use of Ly6G-specific monoclonal antibody to deplete neutrophils in mice, J. Leukoc. Biol. 83 (2007) 64–70. 10.1189/jlb.0407247. [PubMed: 17884993]

[52]. Bronte V, Brandau S, Chen SH, Colombo MP, Frey AB, Greten TF, Mandruzzato S, Murray PJ, Ochoa A, Ostrand-Rosenberg S, Rodriguez PC, Sica A, Umansky V, Vonderheide RH, Gabrilovich DI, Recommendations for myeloid-derived suppressor cell nomenclature and characterization standards, Nat. Commun. 7 (2016) 1–10. 10.1038/ncomms12150.

[53]. Willis AC, Gordon S, Turley L, McKnight AJ, Macfarlane AJ, Dri P, Molecular Cloning of F4/80, a Murine Macrophage-restricted Cell Surface Glycoprotein with Homology to the G-protein-linked Transmembrane 7 Hormone Receptor Family, J. Biol. Chem. 271 (2002) 486–489. 10.1074/jbc.2711.486.

[54]. Murray PJ, Wynn TA, Protective and pathogenic functions of macrophage subsets, Nat. Rev. Immunol. 11 (2011) 723–737. [PubMed: 21997792]

[55]. Banh C, Miah SMS, Kerr WG, Brossay L, Mouse natural killer cell development and maturation are differentially regulated by SHIP-1, Blood. 120 (2012) 4583–4590. 10.1182/blood-2012-04-425009. [PubMed: 23034281]

[56]. Slauenwhite D, Johnston B, Regulation of NKT cell localization in homeostasis and infection, Front. Immunol. 6 (2015). 10.3389/fimmu.2015.00255.

[57]. Jameson SC, Masopust D, Understanding Subset Diversity in T Cell Memory, Immunity. 48 (2018) 214–226. 10.1016/j.immuni.2018.02.010. [PubMed: 29466754]

[58]. Lai L, Alaverdi N, Maltais L, Morse HC, Mouse Cell Surface Antigens: Nomenclature and Immunophenotyping, J. Immunol. 160 (2013) 3861–3868. https://doi.org/160:3861-3868.

[59]. Ogle ME, Segar CE, Sridhar S, Botchwey EA, Monocytes and macrophages in tissue repair: Implications for immunoregenerative biomaterial design, Exp. Biol. Med. 241 (2016) 1084–1097. 10.1177/1535370216650293.

[60]. Malissen B, Tamoutounour S, Henri S, The origins and functions of dendritic cells and macrophages in the skin, Nat. Rev. Immunol. 14 (2014) 417–428. 10.1038/nri3683. [PubMed: 24854591]

[61]. Yanez DA, Lacher RK, Vidyarthi A, Colegio OR, The role of macrophages in skin homeostasis, Pflugers Arch. Eur. J. Physiol. 469 (2017) 455–463. 10.1007/s00424-017-1953-7. [PubMed: 28233123]

[62]. Anderson JM, Rodriguez A, Chang DT, Foreign body reaction to biomaterials, Semin. Immunol. 20 (2008) 86–100. 10.1016/j.smim.2007.11.004. [PubMed: 18162407]

[63]. Landén NX, Li D, Ståhle M, Transition from inflammation to proliferation: a critical step during wound healing, Cell. Mol. Life Sci. 73 (2016) 3861–3885. 10.1007/s00018-016-2268-0. [PubMed: 27180275]

[64]. Franz S, Rammelt S, Scharnweber D, Simon JC, Immune responses to implants - A review of the implications for the design of immunomodulatory biomaterials, Biomaterials. 32 (2011) 6692–6709. 10.1016/j.biomaterials.2011.05.078. [PubMed: 21715002]

[65]. Di Santo JP, Natural Killer Cell Developmental Pathways: A Question of Balance, (2006) 257–288. 10.1146/annurev.immunol.24.021605.090700.

[66]. Jaipersad AS, Lip GYH, Silverman S, Shantsila E, The Role of Monocytes in Angiogenesis and Atherosclerosis, J. Am. Coll. Cardiol. 63 (2014) 1–11. 10.1016/j.jacc.2013.09.019. [PubMed: 24140662]

[67]. Baumgarth N, The double life of a B-1 cell: Self-reactivity selects for protective effector functions, Nat. Rev. Immunol. 11 (2011) 34–46. 10.1038/nri2901. [PubMed: 21151033]

[68]. Duque GA, Descoteaux A, Macrophage cytokines: Involvement in immunity and infectious diseases, Front. Immunol. 5 (2014) 1–12. 10.3389/fimmu.2014.00491. [PubMed: 24474949]

[69]. Ai P, Jaber V, Zhao Y, Wj L, Alzheimer ' s Disease & Parkinsonism Systemic Inflammation in C57BL / 6J Mice Receiving Dietary Aluminum Sulfate; Up-Regulation of the Pro-Inflammatory Cytokines IL-6 and TNF α , C-Reactive Protein (CRP) and miRNA-146a in Blood Serum, 7 (2017). 10.4172/2161-0460.1000403.

[70]. Tracey D, Klareskog L, Sasso EH, Salfeld JG, Tak PP, Tumor necrosis factor antagonist mechanisms of action: A comprehensive review, 117 (2008) 244–279. 10.1016/j.pharmthera.2007.10.001.

[71]. Lotfi P, Tang L, Ko C-Y, Shen J, Nair A, Zhang CC, Biomaterial implants mediate autologous stem cell recruitment in mice, Acta Biomater. 7 (2011) 3887–3895. 10.1016/j.actbio.2011.06.050. [PubMed: 21784181]

[72]. Kode JA, Mukherjee S, Joglekar MV, Hardikar AA, Mesenchymal stem cells: immunobiology and role in immunomodulation and tissue regeneration, Cytotherapy. 11 (2009) 377–391. 10.1080/14653240903080367. [PubMed: 19568970]

[73]. Anderson P, Carrillo-Gálvez AB, García-Pérez A, Cobo M, Martín F, CD105 (Endoglin)-Negative Murine Mesenchymal Stromal Cells Define a New Multipotent Subpopulation with Distinct Differentiation and Immunomodulatory Capacities, PLoS One. 8 (2013) 1–13. 10.1371/journal.pone.0076979.

[74]. Sridharan R, Cameron AR, Kelly DJ, Kearney CJ, Brien FJO, Biomaterial based modulation of macrophage polarization: a review and suggested design principles, Biochem. Pharmacol. 18 (2015) 313–325. 10.1016/j.mattod.2015.01.019.

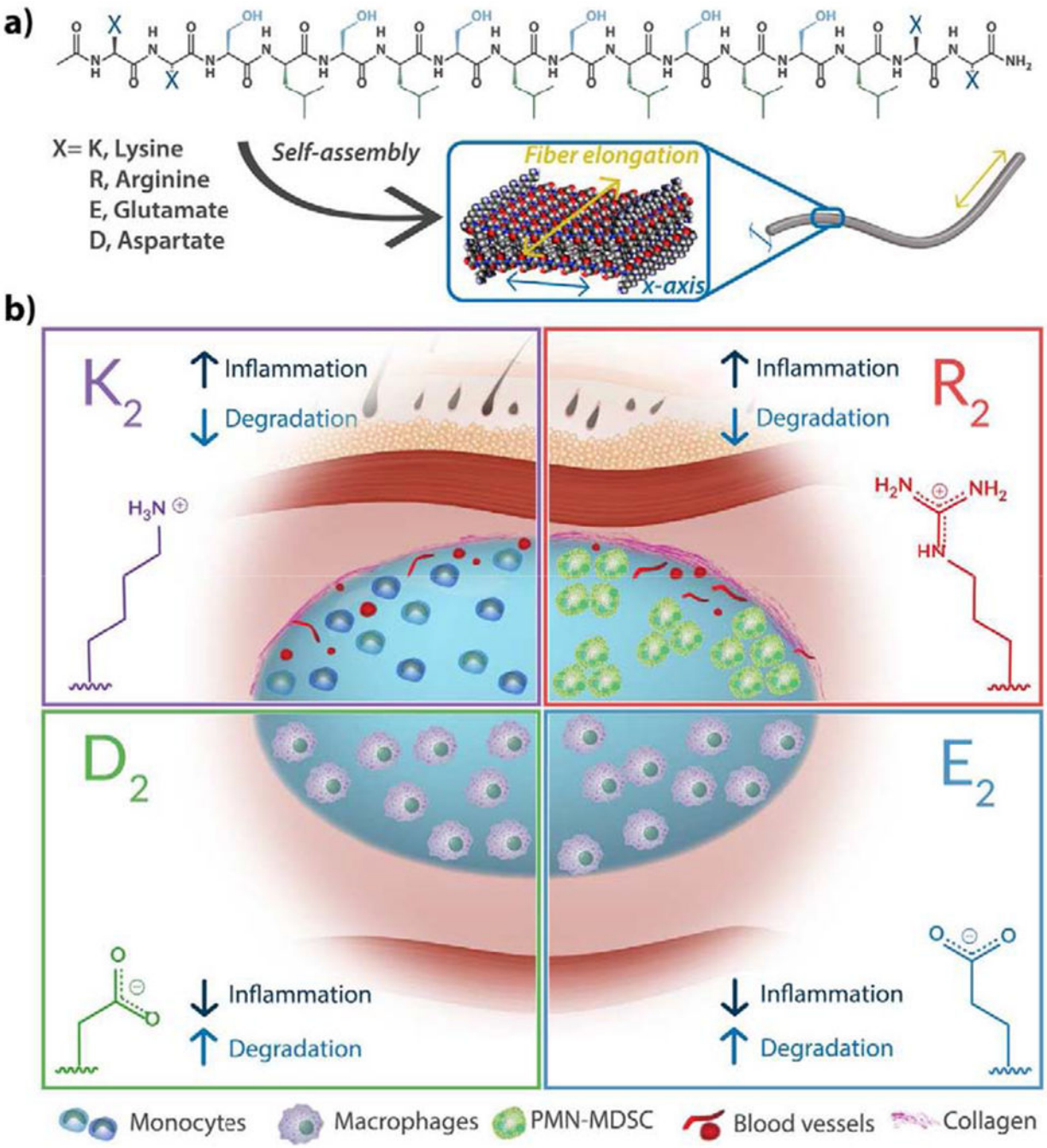

Fig. 1. Self-assembling Multidomain Peptides (MDPs) form a versatile family of nanofibrous scaffold biomaterials.

a) MDP design consists of a core of alternating hydrophilic and hydrophobic residues and ionic charged domains at the N and C-termini. The charged domains can be positively or negatively charged and present different chemical functionalities. b) As described below, the chemistry of MDPs affects the host immune response to the hydrogel: anionic materials bearing deprotonated carboxylic acids (E_2, D_2) provoke a low inflammatory response, characterized by the infiltration of macrophages and fast degradation over a few days. Cationic lysine-based MDP (bearing protonated amines) elicits a mild inflammatory

response that resolves over time, defined by the presence of monocytes, angiogenesis, and mild collagen deposition. Cationic arginine-based MDP (bearing guanidinium ions) provokes a stronger inflammatory response represented by the constant presence of polymorphonuclear myeloid-derived suppressor cells (PMN-MDSC), angiogenesis and high deposition of collagen.

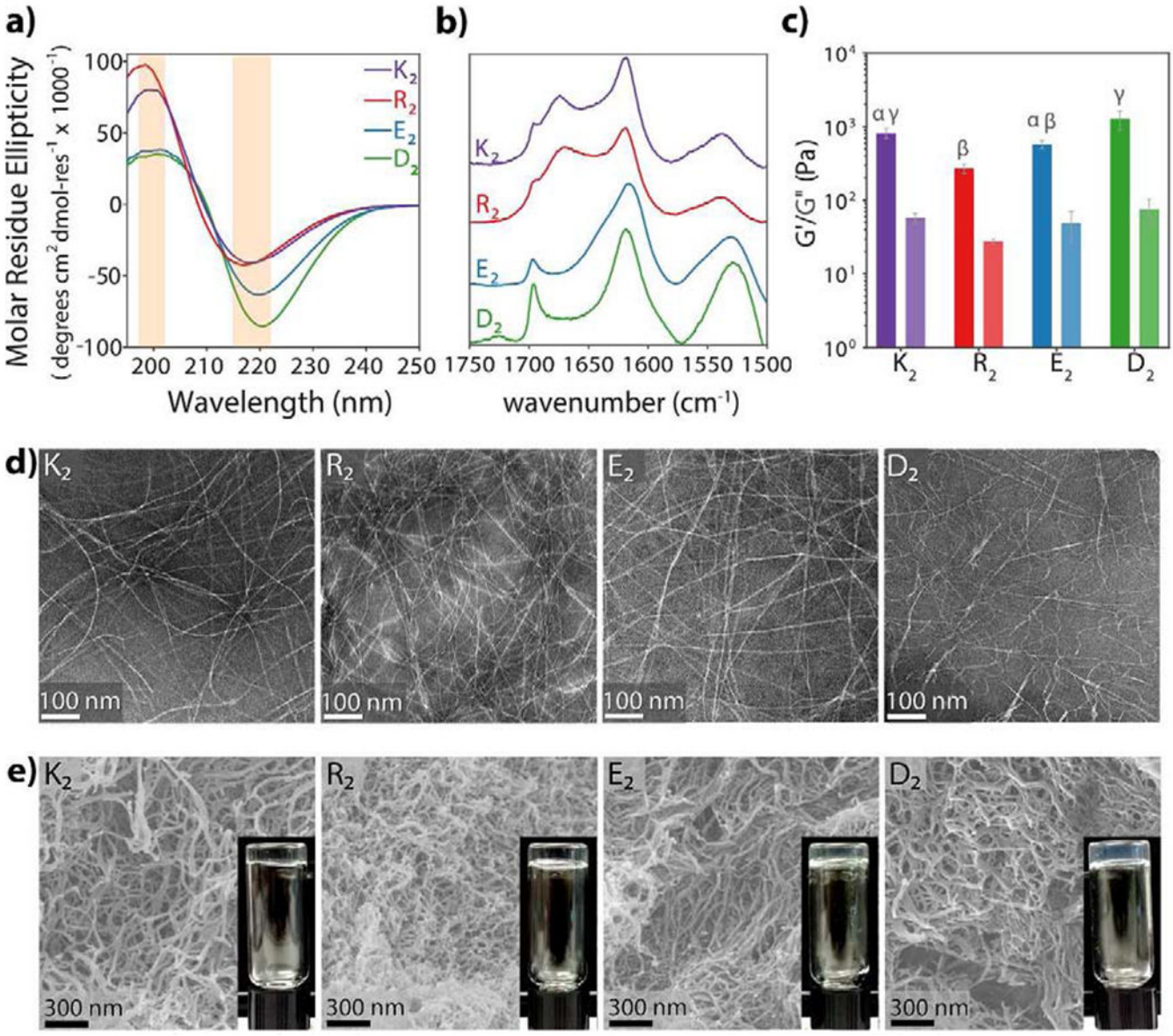

Fig. 2. Structural characterization of multidomain peptides.

a) Circular dichroism spectroscopy of 1% by weight peptide hydrogels shows characteristic β-sheet spectra with minima near 218 nm and maxima near 196 nm. b) Normalized ATR-FTIR spectra of dried peptide films confirm the antiparallel β-sheet secondary structure of all MDPs by the presence of an amide Ia peak at 1620–1630 cm^{-1} and an amide Ib peak near 1695 cm^{-1} c) Viscoelastic properties of MDP hydrogels analyzed by oscillatory rheology. MDPs form soft hydrogels. Error bars represent standard deviation. Different greek letters represent a significant difference, p-value < 0.05. d) MDPs self-assemble into long flexible nanofibers as observed in negative-stained TEM. e) SEM images of peptide hydrogels. Peptide nanofibers are stabilized and physically crosslinked by the presence of ions, forming a highly entangled nanofibrous network and a self-supportive hydrogel.

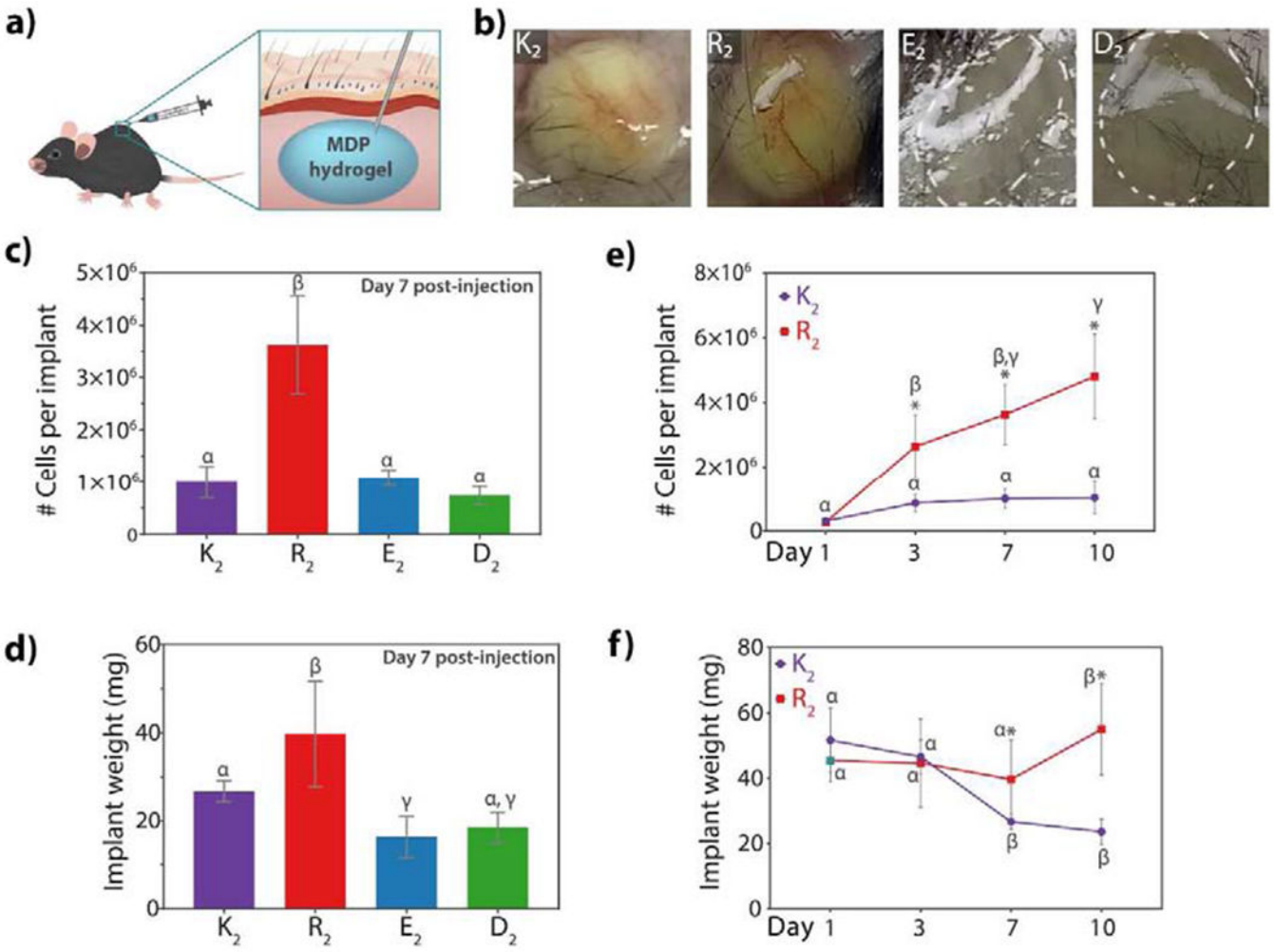

Fig. 3. Gross evaluation of the host immune response to MDP hydrogels.

a) scheme of the mouse subcutaneous injection model used to evaluate the innate host response to all peptides. b) Physical appearance of hydrogel implants three days post-injection. K_2 and R_2 present blood vessels around the implants and a yellow coloration due to the cellular infiltration. E_2 and D_2 do not contain vascularization and appear as clear hydrogel boluses. c) Number of cells obtained from the MDP hydrogel implants at day 7 post-injection. R_2 has a significantly higher cellular infiltration than the other MDPs. d) Weight of the implant seven days after injection. Implant weight is lower in the negative MDPs demonstrating faster degradation. e) Number of cells infiltrating K_2 and R_2 over time. Cellular infiltration in K_2 remains relatively constant at all time points, whereas in R_2 cell number keep increasing even by day 10 post-injection. f) Implant weight of K_2 and R_2 over time. K_2 peptide hydrogel weight decreases by day 7 because of peptide degradation and remodeling. R_2 implant weight remains constant and increases by day 10, suggesting an unresolved inflammatory response. Error bars represent standard deviation. Greek letters represent a significant difference between groups. Symbols represent a significant difference between time points, p-value < 0.05.

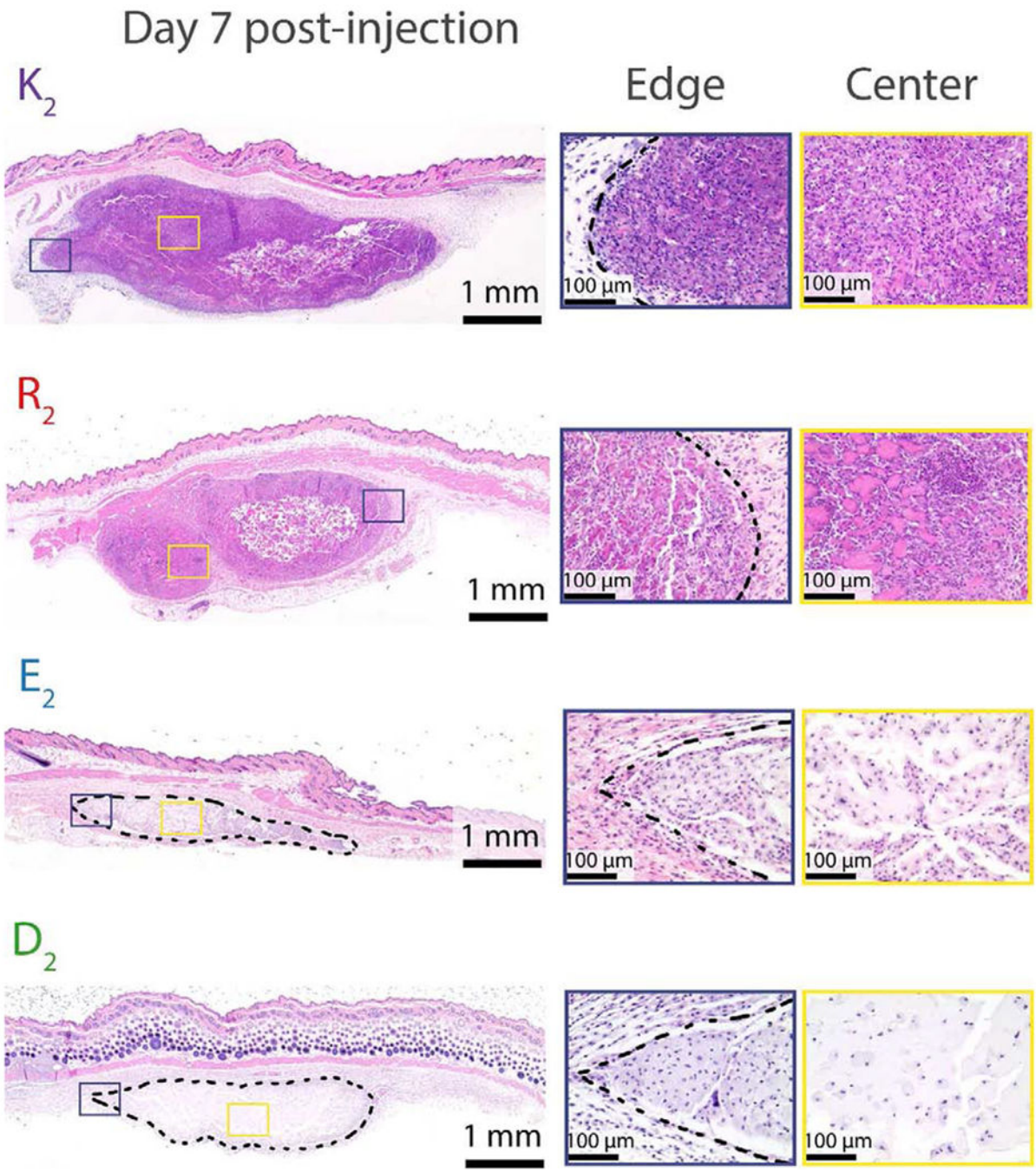

Fig. 4. Hematoxylin & Eosin staining of tissue sections of MDP hydrogel implants at day 7 post-injection.

The purple box represents the area of the implant edge. The yellow box represents the area of the implant center. Dash lines represent the hydrogel in the subcutaneous space. Scale bar: 1 mm. By day 7, all peptides are thoroughly infiltrated by cells. K_2 cell infiltration appears homogeneous, whereas R^2 contains high cell density areas in between hydrogel islets. E_2 and D^2 sizes are considerably reduced in comparison with the positively-charged MDPs.

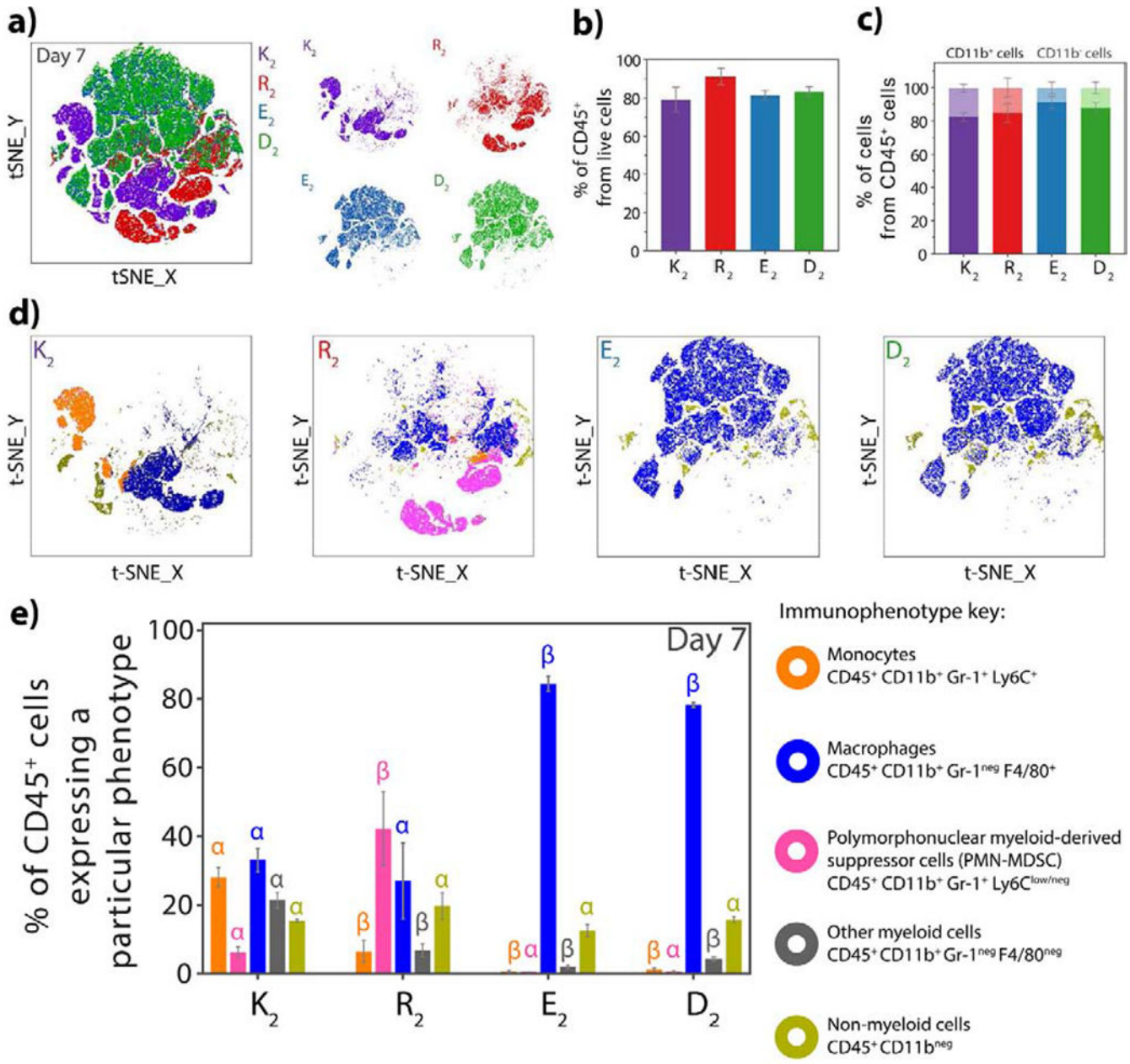

Fig. 5. Phenotypes of cells infiltrating the MDP hydrogels.

a) tSNE clustering of the cellular infiltrate of K_2, R_2, D_2 and E_2 at 7 days post-injection using a 6-color flow cytometry myeloid panel. The positively-charged MDPs, K_2, and R_2 show distinct cell phenotypes while E_2 and D_2 present similar cluster patterns. b) Percentage of $CD45^+$ cells (leukocytes) from live cells that infiltrate the MDP hydrogels at day 7, showing that the materials are infiltrated mostly by immune cells. c) Percentage of myeloid ($CD11b^+$dark color) and non-myeloid ($CD11b^{neg}$ light color) cells from $CD45^+$ present in the peptide hydrogels 7 days post-injection. Myeloid cells are the major population that infiltrates MDP materials. d) tSNE clustering of K_2, R_2, E_2, and D_2 as a representation of the different myeloid populations in each peptide at day 7. e) Percentages of the different cell

populations: monocytes, PMN-MDSCs, macrophages, non-myeloid and other myeloid leukocytes from $CD45^+$ cells that infiltrate the MDP hydrogels at day 7 post-injection. Error bars represent the standard deviation. Greek letters represent a significant difference between groups.

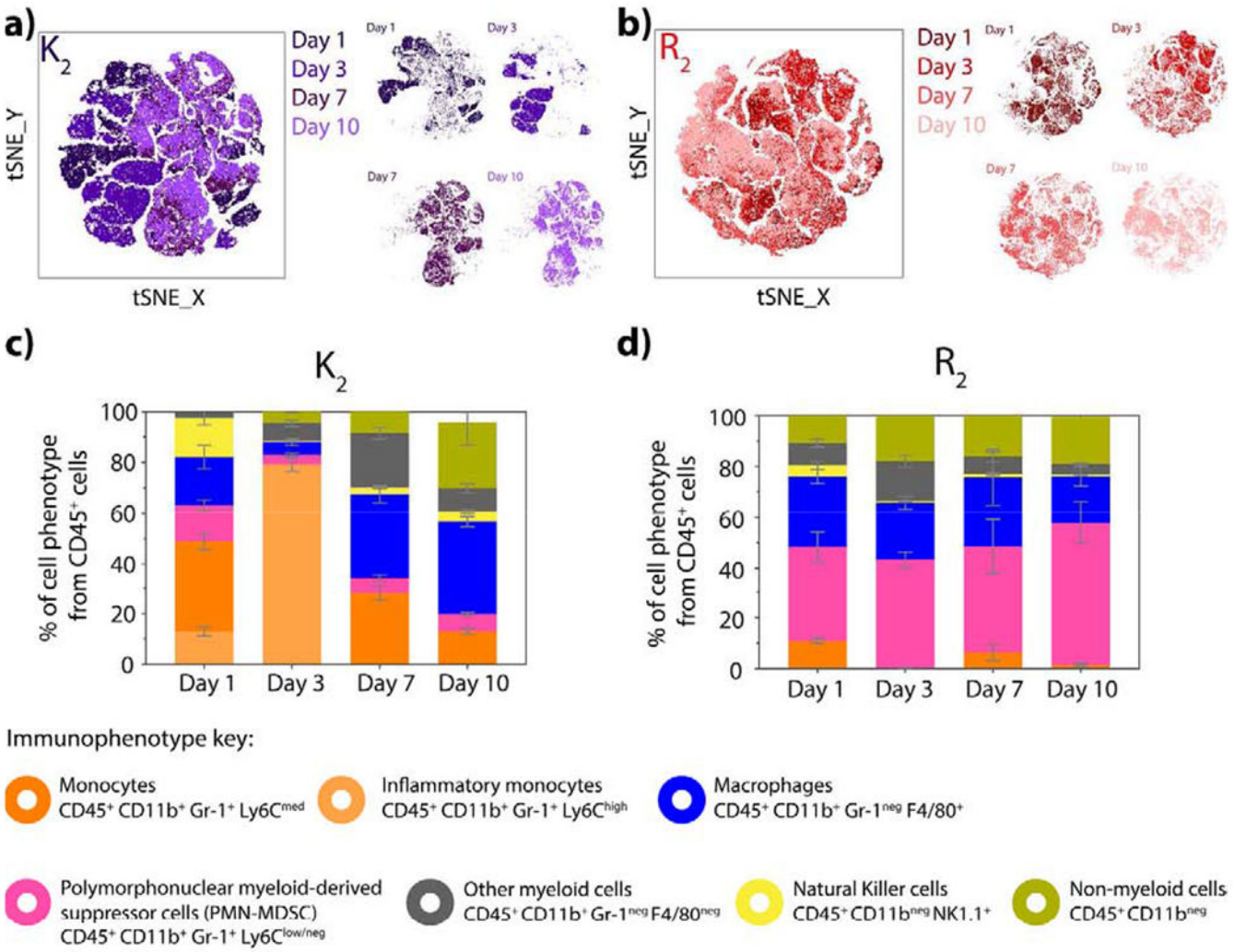

Fig. 6. Time course progression of the infiltrating cell populations for positively-charged MDP hydrogels.

tSNE clustering of cells infiltrating a) K_2 and b) R_2 at day 1, 3, 7 and 10 post-injection using the 6-color myeloid panel. c) Percentage of inflammatory monocytes, monocytes, PMN-MDSC, macrophages, NK cells and other leukocytes from $CD45^+$ cells that infiltrate d) K_2 and R_2 peptide hydrogels at day 1,3, 7 and 10 post-injection. Error bars represent the standard deviation.

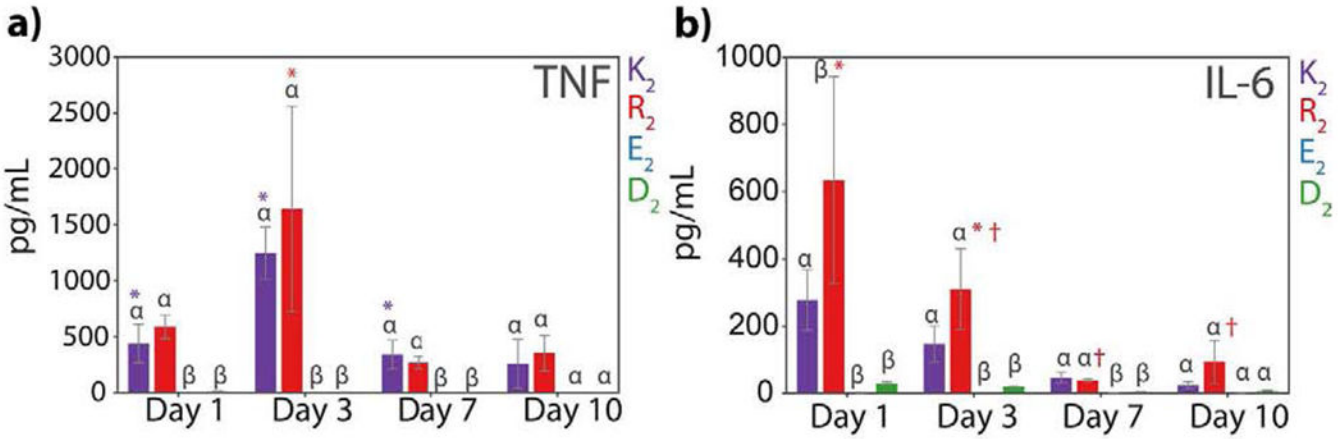

Fig. 7. Quantification of inflammatory cytokines present in the implant lysate.

Quantification of a) TNF and b) IL-6 at day 1, 3, 7, and 10 post-injection of the peptide hydrogel shown in pg/mL in 1mL cell lysis buffer. Error bars represent the standard error of the mean. Greek letters represent a significant difference between groups. Symbols represent a significant difference between time points from the same peptide.

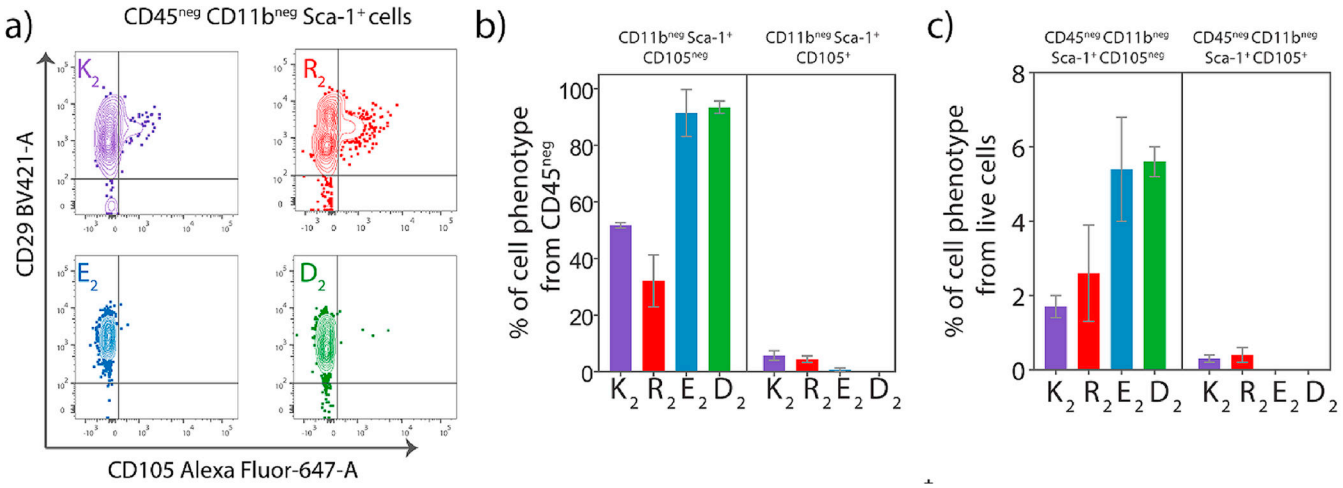

Fig. 8. Presence of Mesenchymal stem cells (CD45^{-} CD11b^{-} Sca-1^{+}) in all peptide hydrogels.

a) Contour plots showing CD105$_{+}$ and CD105^{neg} Sca-1^{+} population from all different MDP peptide hydrogels at day 7 post-injection. Percentage of CD11b^{neg} Sca-1^{+} CD105^{neg} and CD11b^{neg} Sca-1^{+} CD105^{+} MSCs from b) CD45 ^{neg} cells and c) live cells infiltrating the peptide hydrogels at day 7 post-injection.

Table 1.

Summary of the early host immune response to Multidomain Peptide hydrogels displaying different chemical functionalities.

Peptide	K_2	R_2	E_2	D_2
Cellular infiltration	++	+++	+	+
Degradation	++	+	+++	+++
Collagen deposition	++	+++	−	−
Inflammation	++	+++	+	+
Angiogenesis	+	+	−	−
Inflammatory cytokines Main inflammatory cell *	++	+++	+	+
Day 1	Monocytes	PMN-MDSC	−	−
Day 3	Monocytes	PMN-MDSC	Macrophages	−
Day 7	Macrophages	PMN-MDSC	Macrophages	Macrophages
Day 10	Macrophages	PMN-MDSC	−	−
Resolution of inflammation	++	+	+++	+++

* Main inflammatory cell at the specific time point, Phenotypes are: Monocytes: $CD45^+$ $CD11b^+$ $Gr\text{-}1^+$ $Ly6C^{high\text{-}med}$; Polymorphonuclear myeloid-derived suppressor cells (PMN-MDSC): $CD45^+$ $CD11b^+$ $Gr\text{-}1^+$ $Ly6C^{low\text{-}neg}$; Macrophages: $CD45^+$ $CD11b^+$ $Gr\text{-}1^{neg}$ $F4/80^+$.